



# 0D to 3D ZnO nanostructures and their luminescence, magnetic and sensing properties: Influence of pH and annealing



K. Shingange<sup>a,b</sup>, Z.P. Tshabalala<sup>a,b</sup>, B.P. Dhonge<sup>a</sup>, O.M. Ntwaeborwa<sup>b</sup>, D.E. Motaung<sup>a,\*</sup>, G.H. Mhlongo<sup>a,\*</sup>

<sup>a</sup>DST/CSIR National Centre for Nanostructured Materials, Council for Scientific and Industrial Research, Pretoria 0001, South Africa

<sup>b</sup>Department of Physics, University of Free State, Bloemfontein 9300, South Africa

## ARTICLE INFO

### Article history:

Received 30 May 2016

Received in revised form 31 August 2016

Accepted 1 September 2016

Available online 3 September 2016

### Keywords:

Nanostructures

Luminescence

Defects

Magnetic properties

Sensing

## ABSTRACT

Herein, we report on a successful synthesis of ZnO nanostructures with different particle morphologies using the microwave-assisted hydrothermal method. The effect of varying the pH before and after annealing at 450 °C on the particle morphology was evaluated. According to scanning electron microscopy (SEM), electron paramagnetic resonance (EPR), photoluminescence (PL) and Brunauer Emmett Teller (BET) surface area investigations, variation of pH during preparation phase have a significant effect on the morphology, defect structure and surface area of the ZnO nanostructures. Gas sensing performances of the ZnO nanostructures were investigated for methane (CH<sub>4</sub>), carbon monoxide (CO), ammonia (NH<sub>3</sub>) and hydrogen (H<sub>2</sub>) gases at an optimized operating temperature of 250 °C. ZnO sensors displayed comparable responses to these gases owing to variation in their morphology, surface area and porosity as well as defects induced by an increase in pH. The as prepared ZnO based sensors showed the higher response or selectivity to CO gas while the annealed ZnO based sensors showed the higher response or selectivity to NH<sub>3</sub> gas.

© 2016 Elsevier Ltd. All rights reserved.

## 1. Introduction

Preparation of nanosized materials based on ZnO with different morphologies has always been a main focus for several researchers world-wide. The physical and chemical properties of ZnO at the nanoscale level are not easy to predict since they behave completely different from their bulk counterparts [1]. Due to increasing concern over environmental pollution, air quality and occupational safety, much attention has been dedicated to the development of nanostructured ZnO for gas sensing application owing to its high sensitivity of several harmful gases and good thermal and physical stability [2,3]. Furthermore, nanostructured ZnO has been fabricated for the detection of various combustible and toxic gases [4] as well as volatile organic compounds [5]. However, there are a lot of challenges to be overcome that hinder high sensing performance of sensors based on this material including poor sensitivity and selectivity, long response-recovery times and high operating temperature [6]. To overcome these challenges, several approaches have been adopted by different

researchers world-wide including preparation of micro/nanosized ZnO with controlled morphology [5] as well as doping or surface modification of nanostructured ZnO with different elements such as noble metals [7–9], transitional metals [10,11] and by other metal oxides [12–14]. Surface modification of ZnO nanostructures [7,8] has become a hot topic of research recently. However, the ability to fabricate, control and optimize the desired uniform morphology of nanosized ZnO with desired properties is of paramount importance and has generated a lot of interest. Furthermore, control of the shape of ZnO at nanoscale level is rarely achieved and still remains a challenge. Therefore, different innovative methods for the preparation of ZnO nanostructures with specific morphologies for application in gas sensing are still being developed [15–20].

Considering the fact that the sensing mechanism of ZnO is dependent on the surface, its sensing performance rely strongly on the particles morphology, and surface defect states [7,21]. Therefore controlling surface defects has been validated as one of the effective approaches to improve its sensing properties. Based on several experimental findings, manipulation of surface defects can be easily achieved during material processing and annealing treatment [22]. Hence, exploration of experimental techniques such as electron paramagnetic resonance spectroscopy (EPR) and

\* Corresponding authors.

E-mail addresses: [dmotaung@csir.co.za](mailto:dmotaung@csir.co.za) (D.E. Motaung), [gmhlongo@csir.co.za](mailto:gmhlongo@csir.co.za) (G.H. Mhlongo).

photoluminescence (PL) spectroscopy to investigate these defects will provide more insight on their origin making it possible to determine their influence on gas sensing.

Among different approaches that have been developed to prepare ZnO nanostructures with various morphologies [18,23–25], microwave-assisted hydrothermal method which has numerous advantages over other methods such as simplicity of operation, low-energy consumption, control of size, shape and composition [26] has been successfully utilized in this work. Moreover, fabrication of ZnO nanostructures with controlled morphology depend strongly on variation of synthesis conditions such as precursor concentration, reactants pH, reaction time and temperature as well as annealing treatment [17,18,20]. For instance, Singh et al. [19] studied the influence of pH on the morphology of ZnO nanostructures by varying the pH from 8 to 11, and demonstrated transformation of nanorods into nanoparticles at a higher pH of 11. It was further established that the nanoparticles obtained at the pH of 11 showed higher sensing response as compared to other structures obtained at lower pH values. Zhang et al. [20] on the other hand reported morphological changes after ZnO nanostructures were subjected to different annealing temperatures where improved sensitivity to H<sub>2</sub> was observed for annealed ZnO nanorods compared to as prepared ones.

Despite great efforts made, not much effort has been put on establishing the dependence of PL, magnetic and sensing properties on reactants pH and annealing treatment in ZnO nanostructures with various morphologies. In this work, ZnO nanostructures with controlled morphologies from 0D to 3D produced via microwave-assisted method by the variation of pH using NaOH as a morphology directing base precursor is reported. The Influence of pH value before and after annealing on the formation of different morphological structures, defect structure,

porosity and surface area of the ZnO nanostructures was examined in detail. Furthermore, comparative gas sensing measurements among different ZnO nanostructures toward NH<sub>3</sub>, CO, H<sub>2</sub>, and CH<sub>4</sub> were also studied to explore their potential in sensing applications.

## 2. Experimental

### 2.1. Sample preparation

Zinc nitrate hexahydrate ( $\text{Zn}(\text{NO}_3)_2 \cdot 6\text{H}_2\text{O}$ ) and sodium hydroxide (NaOH) were all procured from Sigma-Aldrich and utilized as received without further purification. The reaction solution was prepared by mixing 0.1 M Zinc nitrate hexahydrate ( $\text{Zn}(\text{NO}_3)_2 \cdot 6\text{H}_2\text{O}$ ) and 0.1 M NaOH in separate containers using distilled water as a solvent. These two solutions were then mixed with continuous stirring in one beaker to form a zinc nitrate homogeneous solution. For variation of pH, four separate beakers with each containing the above zinc nitrate solution were prepared. Few drops of NaOH were added on each beaker under vigorous stirring to maintain the pH at 7, 9, 11 and 13, respectively. After being continuously stirred for 15 min, the mixtures were transferred into Teflon vessels, then placed in a microwave oven (EM-G430, 2.45 GHz, maximum output power 1000 W, SANYO Electric, UK) and finally subjected to microwave irradiation power of 150 W for 10 min at 100 °C. After being cooled at room temperature, the white precipitates were collected by centrifugation and washed several times with absolute ethanol and distilled water to get rid of undesirable impurities. The final products were divided into two parts; one part was dried at room temperature and the other was annealed at 450 °C for 2 h. The schematic diagram presented in Fig. 1 shows the proposed formation process of ZnO with different morphologies induced by variation of pH before and after heat treatment

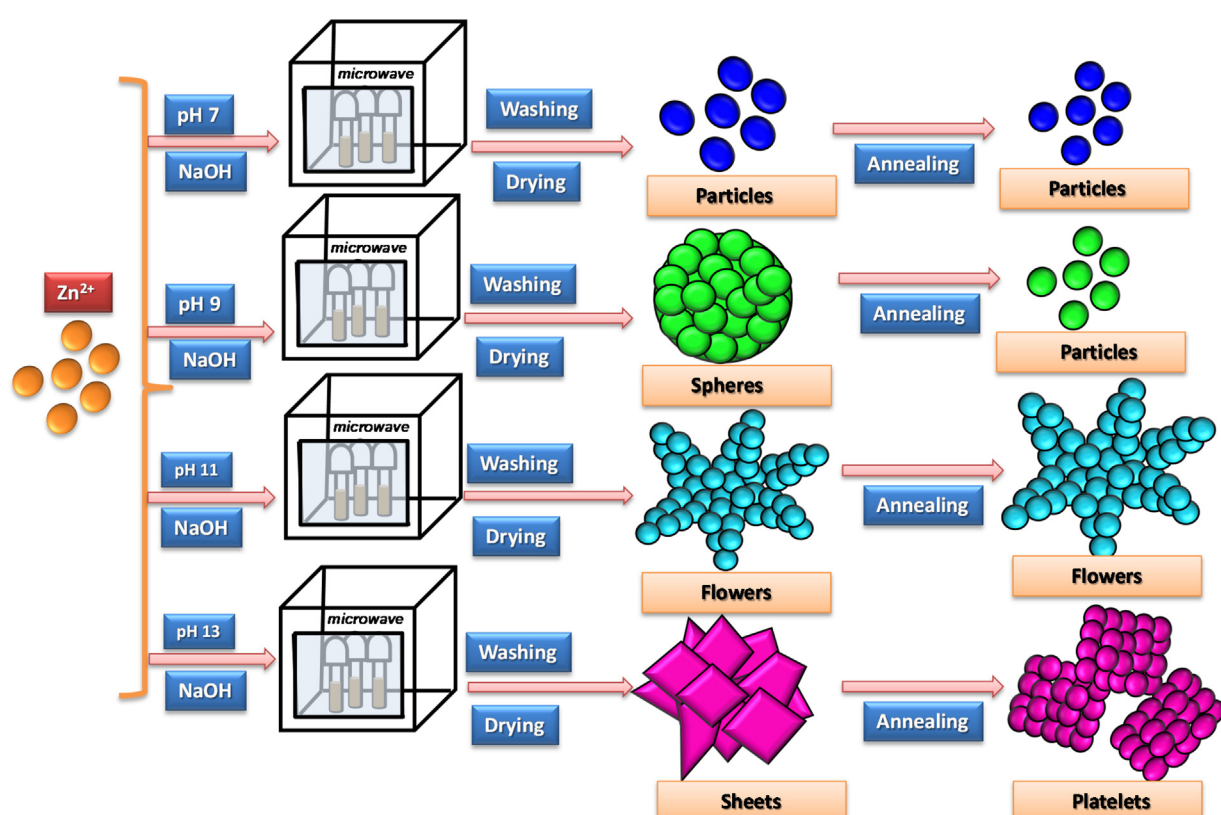


**Fig. 1.** Proposed formation process of ZnO with different morphologies induced by variation of pH.

**Fig. 1** Proposed formation process of ZnO with different morphologies induced by variation of pH.

## 2.2. Sample analysis

The identification of the phases was performed by X-ray diffractometer (XRD) using Panalytical X'pert PRO PW 3040/60 equipped with a Cu-K $\alpha$  ( $\lambda = 0.154$  nm) monochromatized radiation source. The morphology of the synthesized products was examined by scanning electron microscopy (SEM) using ZEIS-AURIGA Focused Ion Beam Scanning Electron Microscopy (FIB-SEM). The specific surface area studies of the nanostructures were measured using a Micrometrics TRISTAR 3000 surface area analyser. Prior to the analysis, the samples were degassed at 150 °C for 12 h under continuous flow of N<sub>2</sub> gas to remove adsorbed incidental impurities. The photoluminescence (PL) spectra were recorded at room temperature following excitation at 325 nm using Jobin-Yvon Nanolog spectrometer. The electron paramagnetic resonance (EPR) spectra were measured at room temperature using a JEOL X-band EPR spectrometer at a constant frequency of 9.4 GHz.

## 2.3. Gas sensor fabrication and testing

Preparation of ZnO based sensors was achieved by dispersing the as prepared and annealed ZnO products in ethanol and drop coating them onto alumina substrates with integrated platinum (Pt) electrodes. The sensing measurements were carried out using a computer-controlled KSGGAS 6S Kenosistec testing station for CH<sub>4</sub>, H<sub>2</sub>, CO and NH<sub>3</sub> gases. A volumetric flow rate of 500 mL min<sup>-1</sup> of synthetic air was maintained during the measurements. Various concentrations ranging from 5 to 100 ppm of each targeted gas in a sensing chamber were achieved by controlling the mass flow rate ratio using a pre-calibrated mass flow meter (MKS Instruments Deutschland GmbH). All the sensor films were first measured at different temperatures (room temperature, 250, 300, 350 and 400 °C) and the films measured at 250 °C revealed enhanced sensing response compared to other temperatures. Therefore, all the sensing measurements were conducted at an optimized operating temperature of 250 °C. The change in the current across the electrode in the presence or absence of target gas was measured using Keithley 6487 Picoammeter/voltage source meter. The gas response of the ZnO based sensors in this case can be defined as  $S = R_a/R_g$  (reducing gases), where  $R_a$  and  $R_g$  were the resistance in air and test gas, respectively.

## 3. Results and discussion

### 3.1. Structural and morphological characterization

In order to establish the phase of the prepared products, XRD analyses were conducted. Fig. 2 shows the representative XRD patterns of the as-prepared and annealed ZnO nanostructures. The diffraction peaks of all the ZnO products are intense and are in good agreement with the wurtzite hexagonal structure of ZnO (JCPDS card no. 36-1451). No diffraction peaks from impurities were observed, indicating that the ZnO nanostructures are of high purity. As shown in Fig. 2(a, b), the diffraction patterns of all the products for both as prepared and annealed were similar, except for the minor variation in peak intensities which could be assigned to the structural changes with pH variation and annealing.

The morphologies of the as-prepared ZnO products examined using SEM are presented in Fig. 3(a–h). It can be seen that for as-prepared products, when the pH of NaOH was 7, spherical particles were formed (see Fig. 3(a, b)). However, with the pH increased to 9, the spherical particles evolved into homogeneously dispersed sphere-like structures as shown in Fig. 3(c). Higher magnification

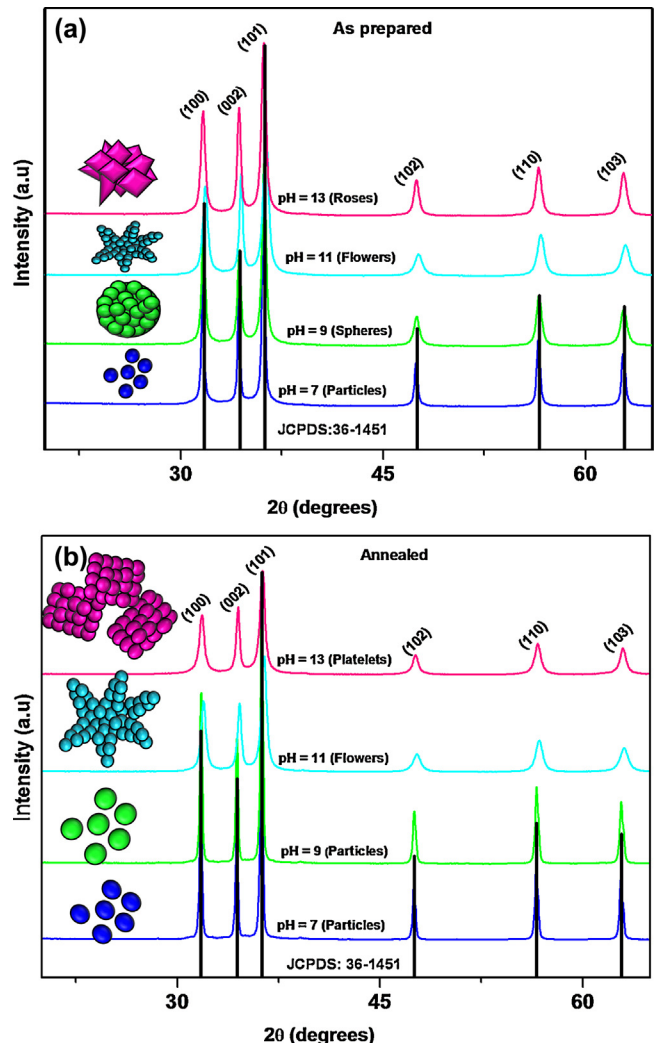


**Fig. 2.** The XRD patterns of the (a) as prepared and (b) annealed ZnO nanostructures obtained after varying pH from 7 to 13 compared with standard wurzite ZnO JCPDS: 36-1451.

of the SEM image in Fig. 3(d) revealed that these sphere-like structures consist of tiny particles which aggregated to form the spherical hierarchical nanostructures.

Fig. 2 The XRD patterns of the (a) as prepared and (b) annealed ZnO nanostructures obtained after varying pH from 7 to 13 compared with standard wurzite ZnO JCPDS: 36-1451.

At a pH value of 11, sphere-like structures were completely transformed into flower-like structures (see Fig. 3(e)). The high resolution SEM image in Fig. 3(f) revealed that every individual flower-like structure is composed of a bunch of nanorods made up of small particles nucleating from one centre forming structures of flower-like hierarchical structure. This structure was not maintained as it evolved into uniform roses-like structures with good dispersion with further increase of pH to 13 (see Fig. 3(g)). A clear observation from HRSEM presented in Fig. 3(h) showed that these roses-like structures are composed of several thin sheets that are stacked close to each other.

When the ZnO products were subjected to high temperature annealing, no obvious morphology change for structures obtained at pH values of 7 and 11 (see Fig. 4(a–d)), except that the particles that were produced at pH 7 became bigger with annealing. However, the sphere-like structures obtained at a pH of 9

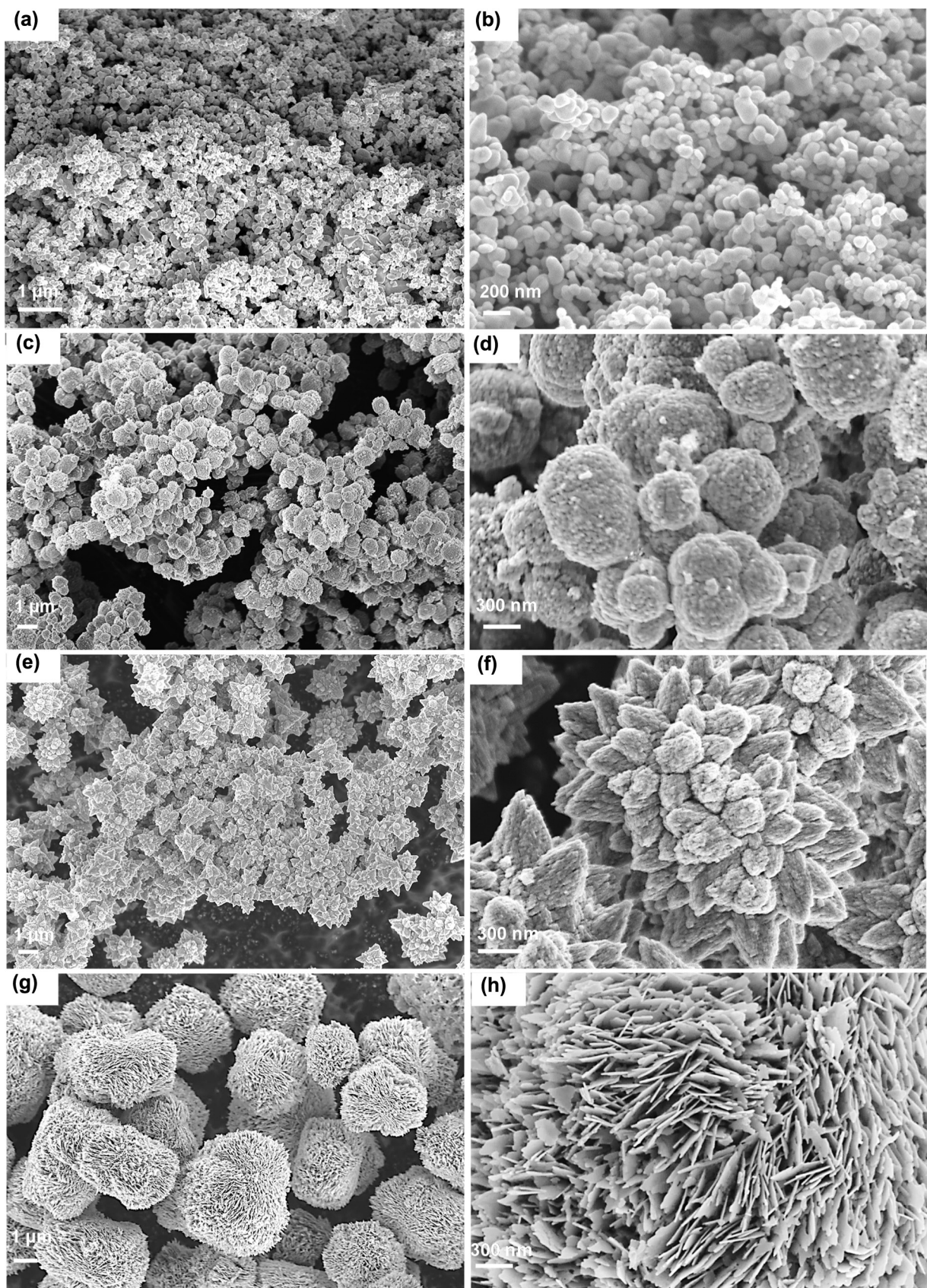


**Fig. 3.** (a–h) SEM images of the as prepared ZnO nanostructures obtained after variation of pH from 7 to 13.

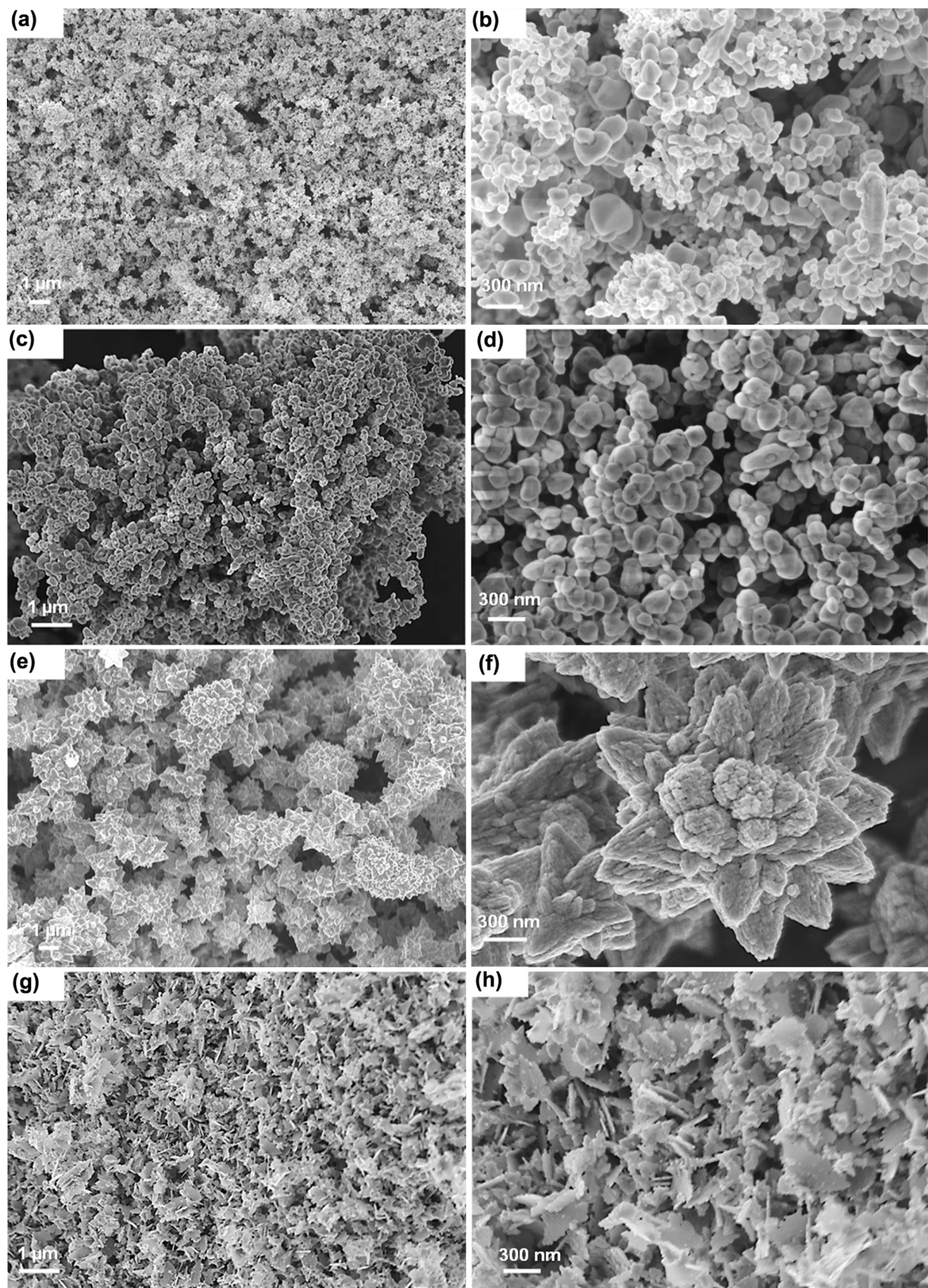


**Fig. 4.** (a–h) SEM images of the annealed ZnO nanostructures obtained after variation of pH from 7 to 13.

transformed into particles with smoother surface after annealing (see Fig. 4(e, f)) while roses-like structures assembled with several thin sheets prior annealing were dissembled into platelets composed by small particles Fig. 4(g, h). It can therefore be concluded based on these SEM observations that variation of pH and annealing treatment plays a significant role in altering the shape of various structures of ZnO.

**Fig. 3(a-h)** SEM images of the as prepared ZnO nanostructures obtained after variation of pH from 7 to 13.

**Fig. 4(a-h)** SEM images of the annealed ZnO nanostructures obtained after variation of pH from 7 to 13.

### 3.2. Brunauer Emmett Teller (BET) analysis

To gain more information about the porous nature of the ZnO structures, BET analysis were carried out. The pore structure parameters such as the surface area, pore size and volume of ZnO nanostructures prior and after annealing are summarized in Table 1. The decrease in BET surface area with increasing pH was observed, except for nanostructures obtained at pH of 13 which showed higher surface compared to the rest of the ZnO structures. Compared to as prepared ZnO nanostructures, a reduction in surface area, pore volume and diameter was observed with annealing as the pH was increased. It can be noticed that of all the nanostructures from this table, the sheets-like and platelet-like structures produced at pH of 13 before and after annealing revealed the largest surface area. Furthermore, the presence of the porous structures in this case indicates the elimination of any solvents and interspaces among the assembled nanoparticles, sheets, flowers, and platelets. As a result, these ZnO nanostructures and hierarchical structures exhibiting higher surface areas and porosity play a significant role in the performance of sensing materials

### 3.3. Photoluminescence (PL) analysis

As mentioned earlier, surface defects are regarded as one of the effective strategies to improve the gas-sensing properties. On the other hand, morphological and structural variations have a considerable effect on the defects structure in ZnO. To verify this effect, the comparison PL spectra of the as prepared and annealed nanostructures were measured at room temperature at an excitation wavelength of 325 nm and are shown in Fig. 5(a, b). As observed in Fig. 5(a), the PL spectra of the as-prepared ZnO nanostructures exhibited considerable differences with varying pH values. For instance, a broad asymmetric feature consisting of two wide bands, the weak one in the blue region and a distinct one in the green region centred at 570 nm was observed. With pH increasing from 7 to 13, the PL intensities of these bands were

shown to increase when the pH was increased up to 11, and then decreased when the pH was further increased to 13. After annealing at 450 °C (see Fig. 5(b)), the green emission band remained strong while the blue one was weakened for ZnO nanostructures obtained at the pH of 7 and 9. Further increase of pH to 11 and 13 led to a significant drop in the PL intensity of the green emission band while the blue emission was intensified. Strong blue emissions were also reported by Motaung et al. [27] and Mhlongo et al. [28] for platelets-like and flower-like structures, respectively.

To understand the origin of individual defects, the observed several peaks were fitted using a Gaussian function for all the spectra including those of the as-prepared (see Fig. 5(c)) and annealed nanostructures (see Fig. 5(d)). The UV emission peaks located at lower wavelengths at 388 nm and 390 nm are usually attributed to the conduction band to valence band (CB-VB) excitonic recombination [15,29]. Violet-blue emissions ranging from 406 to 436 nm can be assigned to zinc interstitials ( $Zn_i$ ) with different charges, including neutral, single and double [30,31]. Blue emissions in the region of 450–460 nm originate from zinc vacancies ( $V_{Zn}$ ) [18,32]. Emission peaks located in the blue-green region from 480 to 555 nm can be ascribed to singly charged oxygen vacancies ( $VO^+$ ) [18,33,34] while those in the yellow (550–610) are mostly attributed to doubly charged oxygen vacancies ( $VO^{++}$ ) [18,33,34]. Orange-red emission peaks between 610 and 750 nm could be due oxygen interstitials ( $O_i$ ) [18,33,35,36].

The enhancement and quenching of the intensity of both green and blue emissions of the as prepared ZnO nanostructures with increasing pH suggest the increase and decrease in the concentration of zinc and oxygen related defects with pH increase. Furthermore, the prominence of the green broad emission indicates that  $VO$  defects exist in large quantities on the ZnO surface for samples produced prior annealing. For structures obtained at lower pH values of 7 and 9 after annealing, the PL spectra were dominated by  $VO$  defects since strong green emissions were observed. In the case of ZnO structures obtained at pH values of 11–13, blue emission was more intense and this indicates that large quantities of  $Zn_i$  were formed on ZnO surface with post-annealing process. The decrease in the PL intensity with annealing in this case can be associated with the decrease in the concentration of both zinc and oxygen related defects on the ZnO surface.

**Fig. 5** Comparison PL spectra of the (a) and (c) as prepared and (b) and (d) annealed ZnO nanostructures after excitation at 325 nm.

### 3.4. Electron paramagnetic (EPR) analysis

To identify and understand the nature of surface defects in ZnO, EPR studies were conducted. Fig. 6(a, b) presents the EPR spectra of the as-prepared and annealed ZnO nanostructures produced at different pH values. Prior to annealing, the EPR spectra (Fig. 6(a)) revealed a broad absorption peak (in the range of 265–370 mT) composed of sharper and narrow peak at 330 mT for all samples except for the pH 11 sample which showed only one broad feature. According to previous studies, the broad EPR signal at approximately 315 mT is associated with ferromagnetic (FM) resonance, while the narrow and sharper one at 330 mT is related to paramagnetic (PM) resonance [18,28]. After annealing, only one broad EPR signal associated with FM could be seen with increasing pH to 11. The PM feature disappeared completely at a higher pH of 13 probably due to improved ordering of the ZnO structure.

The g-factor values for broad EPR signals of the as prepared ZnO nanostructures produced at the pH values of 7, 9, 11, and 13 are 2.0561, 2.0459, 2.0671, and 2.0512, respectively. For annealed ZnO nanostructures, the broad EPR signals exhibited the g-factors of

**Table 1**

Summary of the BET specific surface area, pore volume ( $V_{pore}$ ) and pore diameter ( $d_{pore}$ ) of the ZnO nanostructures before and after annealing.

Sample	As prepared			Annealed		
	Surface area (m <sup>2</sup> /g)	$V_{pore}$ (cm <sup>3</sup> /g)	$d_{pore}$ (nm)	Surface area (m <sup>2</sup> /g)	$V_{pore}$ (cm <sup>3</sup> /g)	$d_{pore}$ (nm)
pH 7 (Particles)	5.62 ± 0.10	0.035	55.31	4.76 ± 0.09	0.013	22.52
pH 9 (Spheres)	5.17 ± 0.11	0.016	48.98	4.29 ± 0.089	0.006	37.70
pH 11 (Flowers)	3.95 ± 0.06	0.014	42.98	1.92 ± 0.04	0.005	51.65
pH 13 (Roses/ Platelets)	28.30 ± 0.24	0.096	24.18	26.49 ± 0.06	0.0739	14.11

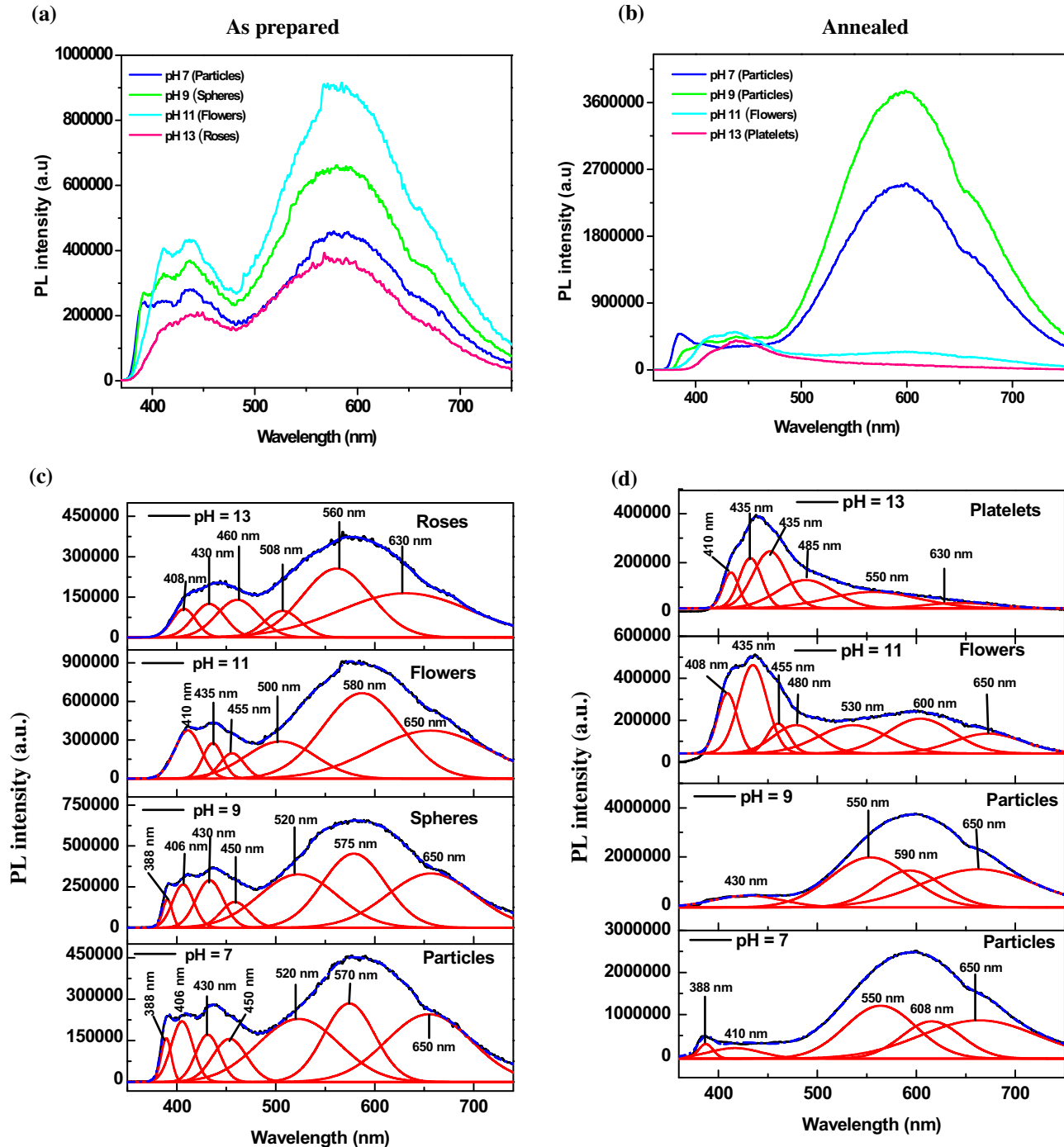


**Fig. 5.** Comparison and deconvoluted PL spectra of the (a), (c) as prepared and (b), (d) annealed ZnO nanostructures after excitation at 325 nm.

2.0407, 2.0512, 2.0725, and 2.0405 for pH values of 7, 9, 11, and 13, respectively. Motaung et al. [27] attributed the broad EPR signals at the g-factors >2.0 to the combination of  $V_{\text{O}}^+$  and  $V_{\text{Zn}}$  defects. Galland et al. [37] and Kakazey et al. [38] also assigned the g-factor values around and close to 2.0 to  $V_{\text{Zn}}$  and  $V_{\text{Zn-Zn}_i}$  complex. Therefore, based on the above experimental findings we speculate that the broad EPR signals at g-factor values greater than 2.0 could be due to combination of  $V_{\text{Zn}}$ ,  $V_{\text{O}}^+$  and  $Zn_i$ .

According to several experimental reports, ferromagnetism in undoped ZnO nanostructures is related to several paramagnetic defects present on the surface of ZnO [27,28]. Furthermore, it is generally accepted that in the absence of dopants in ZnO (undoped),

the magnetism originates from the change in net spins in the d-orbits of Zn ( $3d^9$ ) which can only be promoted by paramagnetic defects such as  $Zn_i$ ,  $V_{\text{Zn}}$ , and  $V_{\text{O}}$ . Based on PL analysis, for the as prepared ZnO nanostructures, the predominant defects are  $V_{\text{O}}$  with different charge states since the as prepared ZnO nanostructures exhibited a strong broad green emission. However, the co-existence of  $V_{\text{O}}$  and  $Zn_i$  is preserved in this case owing to the decrease of the strong green emission with an increase in pH. For annealed ZnO nanostructures,  $V_{\text{O}}$  defects are only predominant for structures obtained at lower pH values (7 and 9) and  $Zn_i$  are of less quantities. For higher pH values of 11 and 13,  $V_{\text{O}}$  defects are strongly quenched and  $Zn_i$  are predominant resulting in intense blue emission.

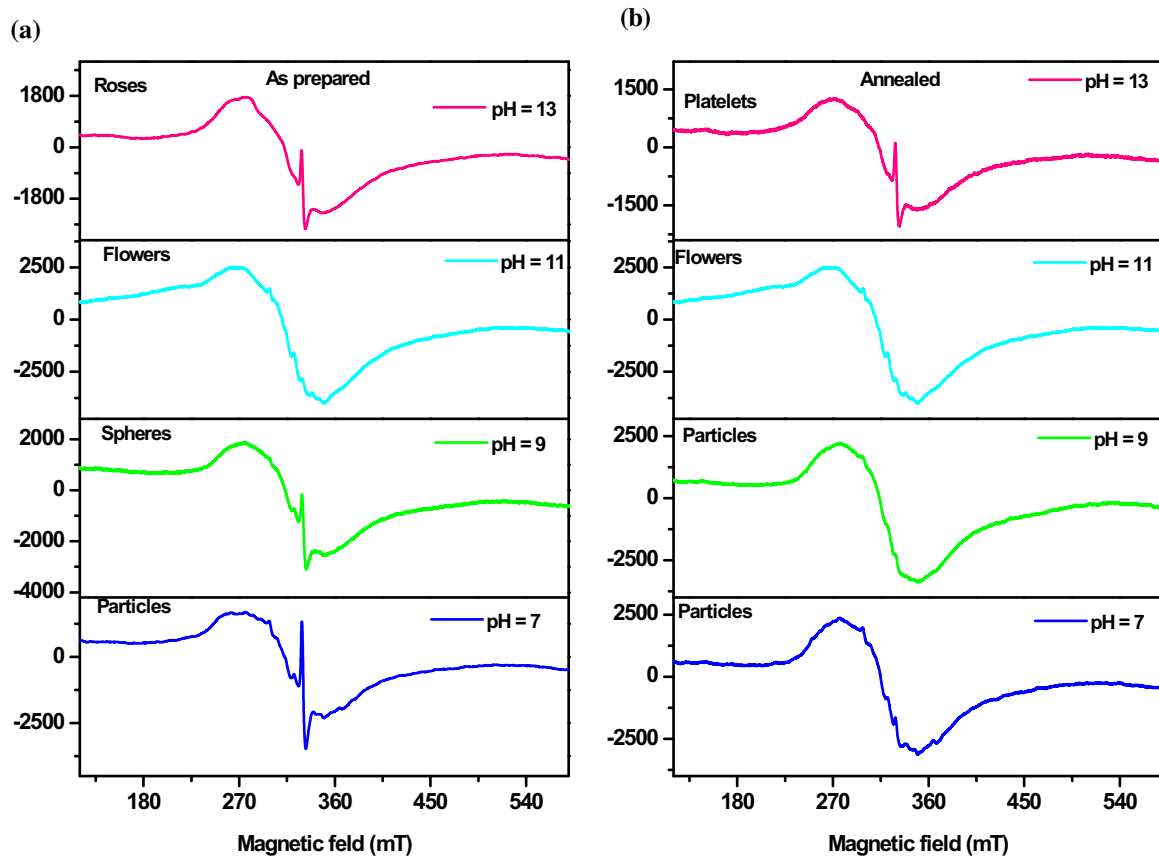


Fig. 6. EPR spectra of the (a) as prepared and (b) annealed ZnO nanostructures obtained after variation of pH from 7 to 13.

It is also important to point out that the FM signal was still maintained irrespective of the enhancement or strong quenching of the strong green emission arising from  $V_O$  while pH varied before and after annealing. Similar behaviour was noticed on the PL emission spectra obtained for structures produced at higher pH values which exhibited strong blue emission due to  $Zn_i$  after annealing. This behaviour confirms the co-existence of various defects contributing to the observed FM [18,27,39] which correlate with the PL studies. It can therefore be concluded based on the correlation studies conducted using EPR and PL that the observed FM in this study originates from the combined effect of  $V_{Zn}$ ,  $V_O^{+}$  and  $Zn_i$  defects. Contribution from  $V_O^{++}$  to FM can be excluded in this case owing to cancellation of two opposite spins [27]. The PM signal is believed to be arising from different magnetic clusters of defects positioned near the surface of ZnO [24].

**Fig. 6** EPR spectra of the (a) as prepared and (b) annealed ZnO nanostructures obtained after variation of pH from 7 to 13.

### 3.5. Gas sensing properties

Gas sensor response of metal oxide based sensors is mainly determined by the interaction between the target gas and oxygen species in the surface of the sensor material. Hence the morphology, surface area and defects are important for gas sensing. The changes in resistance or conductance are caused by various processes which take place both at the surface and in the bulk of a sensing material. To investigate the effect of pH and heat treatment on the gas sensing of ZnO nanostructures, ZnO sensors based on various pH values were tested for different gases including  $CH_4$ , CO,  $NH_3$  and  $H_2$ . Fig. 7(a-d) shows the response characteristics of the as prepared ZnO sensors based on pH 7, 9, 11 and 13 for various concentrations (5–100 ppm) of  $CH_4$ , CO,  $NH_3$  and  $H_2$ .

and  $H_2$  at 250 °C. It is important to note that the response values of all the ZnO based sensors rose rapidly with injection of a specific gas with the corresponding concentration, and then dropped to their initial value after the specific gas was extracted. The response of the sensor based on pH 13 increased linearly with increasing  $CH_4$  concentration until it reached its maximum of 32.9 at 100 ppm (see Fig. 7(a)). The responses of ZnO sensors based on pH 7, 9, and 11 were also shown to increase linearly with the increase of  $CH_4$  concentration at a low concentration range from 5 to 40 ppm while it levelled off and stabilized at a higher  $CH_4$  concentration range from 60 to 100 ppm with maximum responses of 27.7, 27.1, and 16.3, respectively. In addition, these sensors revealed similar responses in the  $CH_4$  concentration ranging from 5 to 80 ppm, except for pH 7 based sensor which showed higher response from 5 to 10 ppm. After exposing the nanostructures to CO (see Fig. 7(b)), pH 7 and 13 based sensors exhibited a nearly linear response increase with increasing CO concentration with a maximum of 159.7 and 136.6 at 100 ppm, respectively. ZnO sensors based on pH 11 and 9 showed a gradual increase in response up to 40 ppm, then stabilized in the CO concentration range from 60 to 100 ppm. It is also important to note that these sensors displayed similar response from 5 to 100 ppm of CO with the pH 7 based sensor revealing a slightly higher response from 40 to 100 ppm as compared to its counterparts. With exposure to  $NH_3$  (see Fig. 7(c)), the pH 7 based sensor revealed higher response from 5 to 100 ppm of  $NH_3$  with a maximum of 220.3 at 100 ppm which is 8 times higher than the rest of the sensors. Furthermore, a linear increase with an increase in  $NH_3$  concentration from 5 to 100 ppm was displayed by all ZnO based sensors. Upon exposure to  $H_2$ , both the pH 9 and 11 sensors showed a maximum response of 90.1 and 85.5 at 5 ppm, respectively while the pH 13 revealed a maximum

### As prepared

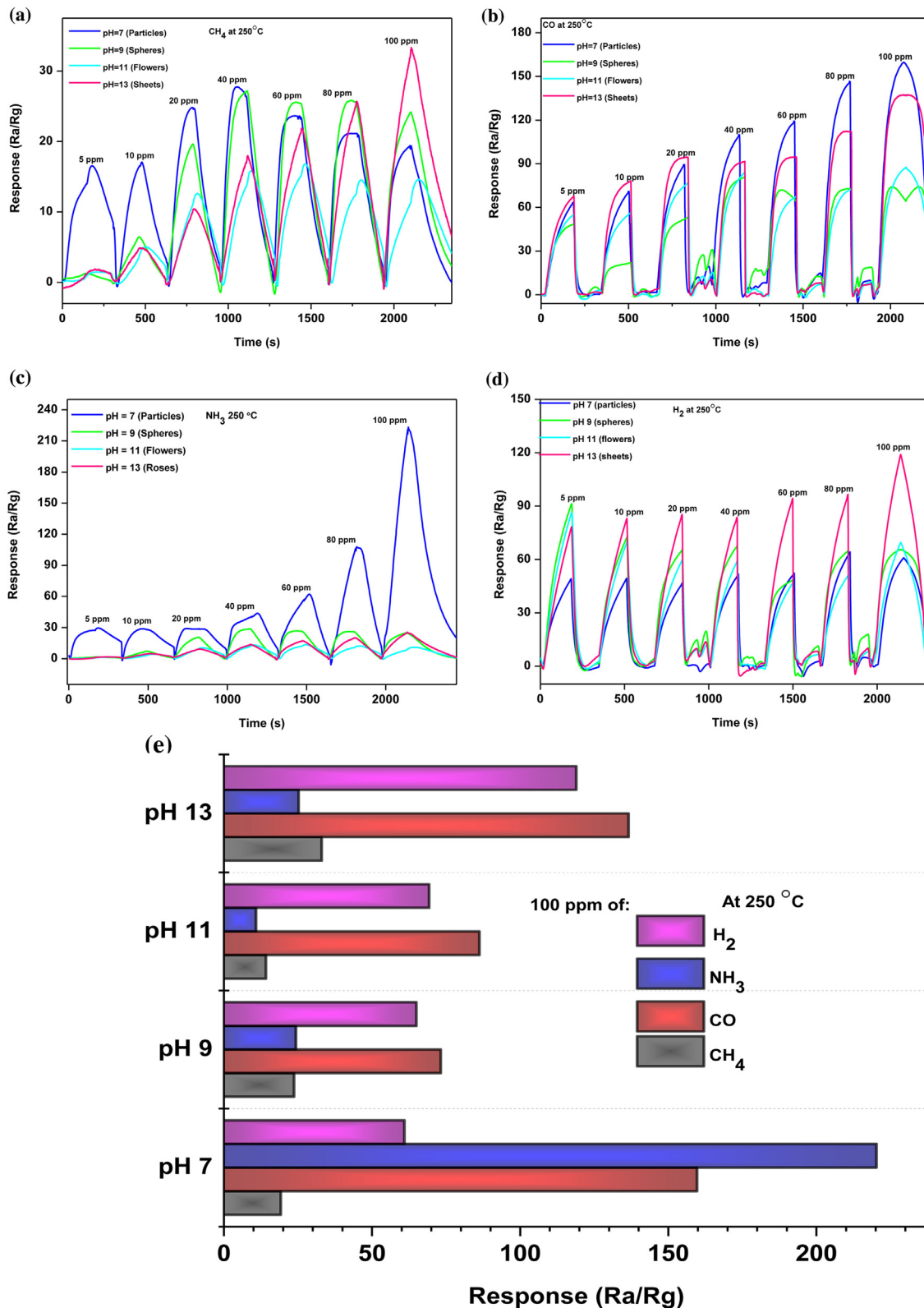


**Fig. 7.** Response curves of the as prepared ZnO based sensors to different concentrations of (a)  $\text{CH}_4$ , (b) CO, (c)  $\text{NH}_3$  and (d)  $\text{H}_2$ . The histogram (e) shows the response of the as prepared ZnO to 100 ppm of different gases.

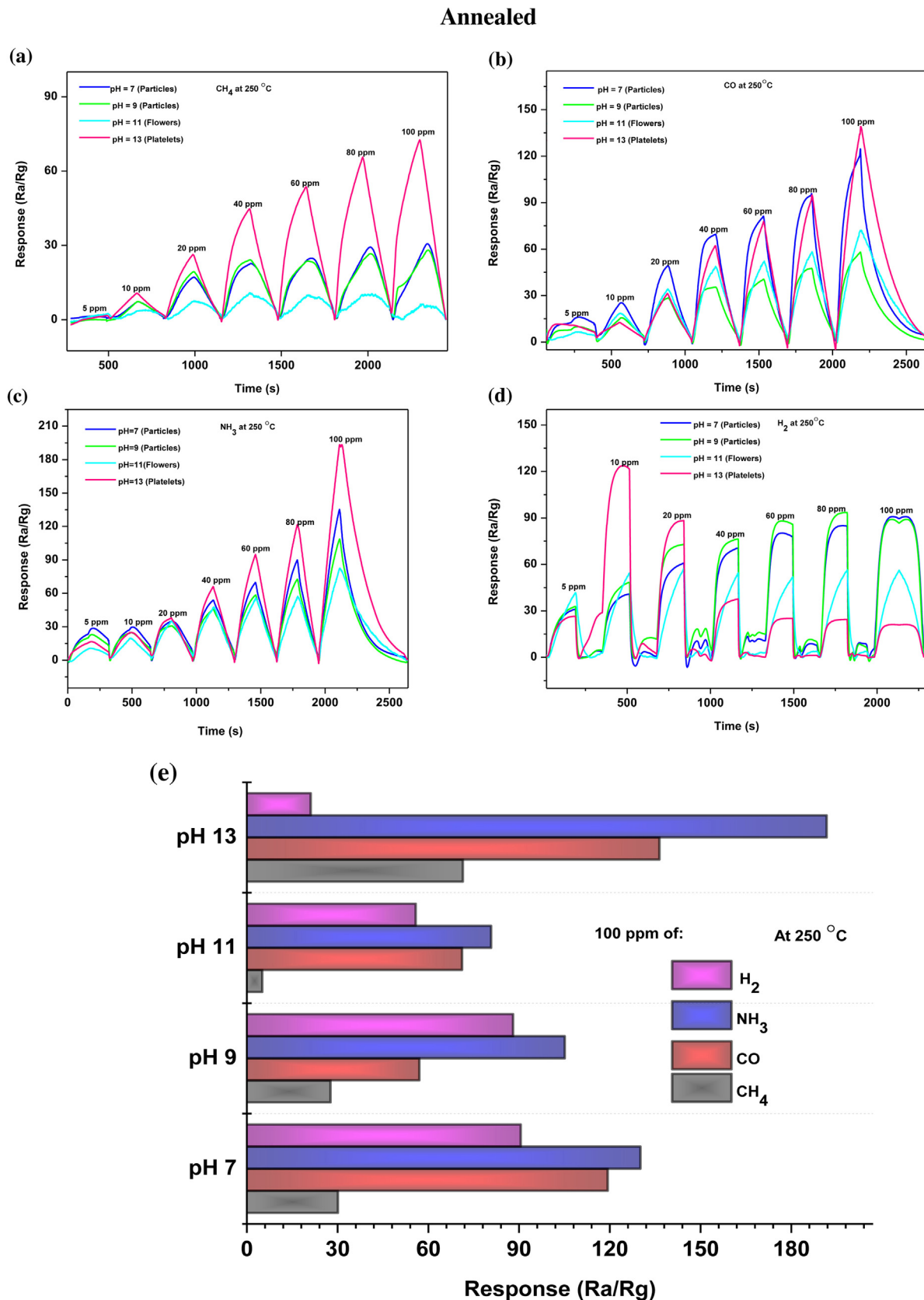


**Fig. 8.** Response curves of the ZnO based sensors, after annealing, to different concentrations of (a)  $\text{CH}_4$ , (b)  $\text{CO}$ , (c)  $\text{NH}_3$  and (d)  $\text{H}_2$ . The histogram (e) shows the response of the as prepared ZnO to 100 ppm of different gases.

of 118.9 at 100 ppm. Additionally, pH 13 based sensors displayed higher response from 10 to 100 ppm compared to the rest of the sensors whereas that of the pH 7 based sensor was found to be stable from 5 to 100 ppm. Based on these observations, it is clear that all the as-prepared ZnO based sensors showed high response upon exposure to CO except for the pH 7 based sensors which displayed its high response to NH<sub>3</sub>. This trend can be clearly seen from Fig. 7(e) where the gas sensing response of various ZnO based sensors to 100 ppm of CH<sub>4</sub>, CO, NH<sub>3</sub> and H<sub>2</sub> at 250 °C is presented.

**Fig. 7:** Response curves of the as prepared ZnO based sensors to different concentrations of (a) CH<sub>4</sub>, (b) CO, (c) NH<sub>3</sub> and (d) H<sub>2</sub>. The histogram (e) shows the response of the as prepared ZnO to 100 ppm of different gases.

Annealing of the as prepared ZnO nanostructures is important in this regard considering the fact that long-term operation of a sensor material at elevated temperatures will lead to subsequent sintering thus altering microstructural properties of the ZnO nanostructures with time. Therefore, to improve strength, durability and stability of the synthesized ZnO nanostructures, the as prepared nanostructures were annealed at 450 °C and gas response behaviour towards various gases including CO, NH<sub>3</sub>, H<sub>2</sub>, and CH<sub>4</sub> were studied at an optimized operating temperature of 250 °C. Fig. 8(a–d) presents the response curves of the annealed ZnO sensors based on pH 7, 9, 11 and 13. With exposure of the sensors to CH<sub>4</sub>, CO and NH<sub>3</sub>, the linear increase in response from low to high concentration ranging from 5 to 100 ppm was observed. All the sensors revealed their maximum response at 100 ppm with the pH 13 based sensor showing higher response to CH<sub>4</sub> and NH<sub>3</sub> as compared to other sensors. Both pH 7 and 13 displayed higher response to CO with similar intensities. With exposure to H<sub>2</sub>, pH 7 and 9 sensors exhibited a gradual increase with increasing H<sub>2</sub> concentration up to 20 ppm, and then stabilized with further increase in concentration from 20 to 100 ppm. The response of the ZnO sensor based on pH 13 was shown to drastically increase from 5 to 10 ppm, then decreased with an increase in H<sub>2</sub> concentration to 20 ppm and finally stabilized with further increase in concentration to 100 ppm. It was also noticed that all the annealed ZnO based sensors exhibited high response when exposed to NH<sub>3</sub>. This observation can be clearly seen in Fig. 8(e) where the gas sensing response of various ZnO based sensors to 100 ppm of CH<sub>4</sub>, CO, NH<sub>3</sub> and H<sub>2</sub> at 250 °C is presented.

**Fig. 8:** Response curves of the ZnO based sensors, after annealing, to different concentrations of (a) CH<sub>4</sub>, (b) CO, (c) NH<sub>3</sub> and (d) H<sub>2</sub>. The histogram (e) shows the response of the as prepared ZnO to 100 ppm of different gases.

Based on the above observations, it is obvious that there is variation in response values of the ZnO sensors based on various pH values prior to and after annealing. However, both particles and roses-like or platelet-like structures obtained at pH values of 7 and 13 revealed a better sensing performance towards certain gases before and after annealing. This behaviour can be explained in terms of the differences in morphology, surface defects and surface area. The gas sensing properties are known to be greatly affected by morphology and size of the sensing material. On the one hand, particle morphology influences the surface area of the sensing materials. Larger surface area means more active sites for gas molecules adsorption and desorption. This may then attract more electrons from the bulk of ZnO making the sensor having higher surface area more sensitive to the tested gases. SEM observations showed structural changes from 0D to 3D where nanoparticles were transformed to flower-like, sphere-like, and roses-like or platelet-like hierarchical structures assembled by nanoparticles (sheets for roses-like structures) with rich-pore structures among them with increasing pH prior and after annealing. These hierarchical structures are expected to not only provide efficient

and fast diffusion of gas molecules but to also exhibit large surface area which will provide more active sites for adsorption of gas molecules thus improving the gas sensing performance. Likewise, 0D nanoparticles are useful for gas sensitivity enhancement owing to their high surface area, though, smaller mesoporous may sometimes hinder the diffusion of gas molecules into the inner part of the secondary particles which can ultimately lower or delay the sensing response. Moreover, BET surface area analyses revealed higher surface area for roses-like or platelet-like hierarchical structures obtained at the pH of 13 exhibited followed by particles produced at the pH of 7 before and after annealing as compared to the rest of the structures. This also explains the observed better sensing performance exhibited by these structures when exposed to certain gases prior and after annealing treatment.

As another important factor that may promote variation in responses of the ZnO sensors, surface defects, such as Zn<sub>i</sub> and V<sub>O</sub>, in ZnO nanostructures act as electron donors in ZnO to supply more electrons to the conduction band of ZnO. Thus, the presence of Zn<sub>i</sub> and V<sub>O</sub> in larger quantities will promote greater absorptions of oxygen without dropping the expansion level of ZnO nanostructures depletion layer leading to further increase of response. In this study, PL and EPR studies revealed high concentration of V<sub>O</sub> and/or Zn<sub>i</sub> defects on the surface of ZnO nanostructures before and after annealing. Existence of such defects in large amounts provide more channels for transportation of target gas molecules and formation of oxygen species thus contributing to the observed variation in sensor responses.

We also noticed that annealing of ZnO nanostructures caused a slight decrease in sensor response (except for NH<sub>3</sub> selective gas) for all the ZnO sensors to the tested gases. This behaviour could be arising from the reduction in the surface area and porosity of the ZnO structures with annealing treatment as revealed by BET surface area analysis. This suggests that higher temperature annealing induced an obvious decrease of surface adsorption positions and reacting area for oxygen and target gases. It is also important to mention that annealing at high temperatures results in the rapid decrease in the concentration of the surface defects in ZnO. For example, the PL and EPR studies revealed a decrease in the PL and EPR signals of the ZnO nanostructures with annealing confirming the decrease in the concentration of surface defects including Zn<sub>i</sub> and V<sub>O</sub>. Reduction in the concentration of Zn<sub>i</sub> and V<sub>O</sub> donor defects in the surface of ZnO means less adsorption of oxygen and this lowers the sensor response.

#### 4. Conclusion

As-prepared and annealed ZnO nanostructures with different morphologies were successfully synthesized using the microwave-assisted hydrothermal method while varying the pH n. Structural examination revealed transformation in the particle shape of the as prepared ZnO nanostructures from spherical particles to roses-like structures with variation of pH from 7 to 13. The particle morphologies of these various ZnO nanostructures obtained after pH variation were found to evolve again with annealing except for particles and flower-like structures obtained at pH of 7 and 11, respectively, which maintained their shapes. The BET measurements revealed a drop in surface area and porosity after annealing. Photoluminescence (PL) and electron paramagnetic resonance (EPR) analyses revealed that increasing pH caused variation in the concentration of Zn<sub>i</sub> and V<sub>O</sub> defects which dominated blue and green emissions respectively. Variation in surface area, morphology as well as surface defects caused by change of pH could be the main reason for the observed variation of ZnO sensors responses upon exposure to various concentrations of CO, CH<sub>4</sub>, NH<sub>3</sub> and H<sub>2</sub> at 250 °C for both the as-prepared and annealed ZnO structures. The

as prepared sensors showed high response to CO, whereas the annealed nanostructures showed the highest response to NH<sub>3</sub>.

## Acknowledgements

This work was supported by the Department of Science and Technology, the Council for Scientific and Industrial Research (HGER27S). We would also like to acknowledge the National Centre for Nanostructured Materials (NCNSM) characterization facility.

## References

- [1] W. Guo, T. Liu, H. Zhang, R. Sun, Y. Chen, W. Zeng, Z. Wang, *Sens. Actuators B* 166 (2012) 492–499.
- [2] X. Zhou, Q. Xue, H. Chen, C. Liu, *Phys. E Low Dimens. Syst. Nanostruct.* 42 (2010) 2021–2025.
- [3] M. Suchea, S. Christoulakis, K. Moschovis, N. Katsarakis, G. Kiriakidis, *Thin Solid Films* 515 (2006) 551–554.
- [4] E. Comini, G. Faglia, G. Sberveglieri, Z. Pan, Z.L. Wang, *Appl. Phys. Lett.* 81 (2002) 1869–1871.
- [5] N.F. Hamedani, A.R. Mahjoub, A.A. Khodadadi, Y. Mortazavi, *Sens. Actuators B* 156 (2011) 737–742.
- [6] G.K. Mani, J.B.B. Rayappan, *Mater. Lett.* 158 (2015) 373–376.
- [7] P. Rai, Y.-S. Kim, H.-M. Song, M.-K. Song, Y.-T. Yu, *Sens. Actuators B* 165 (2012) 133–142.
- [8] C. Liewhiran, S. Phanichphant, *Sensors* 7 (2007) 1159–1184.
- [9] G.H. Mhlongo, D.E. Motaung, H.C. Swart, *Mater. Lett.* 160 (2015) 200–205.
- [10] L. Peng, P. Qin, Q. Zeng, H. Song, M. Lei, J.J. Mwangi, D. Wang, T. Xie, *Sens. Actuators B* 160 (2011) 39–45.
- [11] Q. Xiao, T. Wang, *Mater. Res. Bull.* 48 (2013) 2786–2791.
- [12] N. Han, X. Wu, D. Zhang, G. Shen, H. Liu, Y. Chen, *Sens. Actuators B* 152 (2011) 324–329.
- [13] J. Kim, W. Kim, K. Yong, *J. Phys. Chem. C* 116 (2012) 15682–15691.
- [14] X. Jia, H. Fan, *Mater. Res. Bull.* 45 (2010) 1496–1500.
- [15] F. Gu, D. You, Z. Wang, D. Han, G. Guo, *Sens. Actuators B* 204 (2014) 342–350.
- [16] W. Guo, T. Liu, R. Sun, Y. Chen, W. Zeng, Z. Wang, *Sens. Actuators B* 178 (2013) 53–62.
- [17] S. Hussain, T. Liu, M. Kashif, L. Lin, S. Wu, W. Guo, W. Zeng, U. Hashim, *Mater. Sci. Semicond. Process.* 18 (2014) 52–58.
- [18] K. Shingange, G. Mhlongo, D. Motaung, O. Ntwaeaborwa, *J. Alloys Compd.* 657 (2016) 917–926.
- [19] O. Singh, M.P. Singh, N. Kohli, R.C. Singh, *Sens. Actuators B* 166 (2012) 438–443.
- [20] J.-j. Zhang, E.-j. Guo, L.-p. Wang, H.-y. Yue, G.-j. Cao, S. Liang, *Trans. Nonferrous Metals Soc. China* 24 (2014) 736–742.
- [21] X.-G. Han, H.-Z. He, Q. Kuang, X. Zhou, X.-H. Zhang, T. Xu, Z.-X. Xie, L.-S. Zheng, *J. Phys. Chem. C* 113 (2008) 584–589.
- [22] H.S. Kang, J.S. Kang, J.W. Kim, S.Y. Lee, *J. Appl. Phys.* 95 (2004) 1246–1250.
- [23] J. Bhat, A. Patil, N. Swami, B. Mulimani, B. Gayathri, N. Deshpande, G. Kim, M. Seo, Y. Lee, *J. Appl. Phys.* 108 (2010) 043513.
- [24] G. Mhlongo, D. Motaung, I. Kortidis, N. Mathe, O. Ntwaeaborwa, H. Swart, B. Mwakikunga, S. Ray, G. Kiriakidis, *Mater. Chem. Phys.* 162 (2015) 628–639.
- [25] T. Terasako, M. Yagi, M. Ishizaki, Y. Senda, H. Matsuura, S. Shirakata, *Surf. Coat. Technol.* 201 (2007) 8924–8930.
- [26] R. Majithia, J. Speich, K.E. Meissner, *Materials* 6 (2013) 2497–2507.
- [27] D. Motaung, G. Mhlongo, S. Nkosi, G. Malgas, B. Mwakikunga, E. Coetsee, H. Swart, H. Abdallah, T. Moyo, S. Ray, *ACS Appl. Mater. Interfaces* 6 (2014) 8981–8995.
- [28] G.H. Mhlongo, D.E. Motaung, S.S. Nkosi, H. Swart, G.F. Malgas, K.T. Hillie, B.W. Mwakikunga, *Appl. Surf. Sci.* 293 (2014) 62–70.
- [29] M. Chen, Z. Wang, D. Han, F. Gu, G. Guo, *J. Phys. Chem. C* 115 (2011) 12763–12773.
- [30] S. Panda, C. Jacob, *Appl. Phys. A* 96 (2009) 805–811.
- [31] V. Kumar, H. Swart, M. Gohain, V. Kumar, S. Som, B. Bezuidenhoudt, O. Ntwaeaborwa, *Ultrason. Sonochem.* 21 (2014) 1549–1556.
- [32] P. Rai, J.-N. Jo, I.-H. Lee, Y.-T. Yu, *Mater. Chem. Phys.* 124 (2010) 406–412.
- [33] B. Panigrahy, M. Aslam, D.S. Misra, M. Ghosh, D. Bahadur, *Adv. Funct. Mater.* 20 (2010) 1161–1165.
- [34] H. Gao, D. Gao, G. Yang, J. Zhang, J. Zhang, Z. Shi, D. Xue, *Phys. Status Solidi A* 208 (2011) 2454–2459.
- [35] G. Mhlongo, D. Motaung, I. Kortidis, N. Mathe, O. Ntwaeaborwa, H. Swart, B. Mwakikunga, S. Ray, G. Kiriakidis, *Mater. Chem. Phys.* 162 (2015) 628–639.
- [36] U. Pal, J.G. Serrano, P. Santiago, G. Xiong, K. Ucer, R. Williams, *Opt. Mater.* 29 (2006) 65–69.
- [37] D. Galland, A. Herve, *Solid State Commun.* 14 (1974) 953–956.
- [38] M. Kakazey, M. Vlasova, M. Dominguez-Patiño, G. Dominguez-Patiño, G. Gonzalez-Rodriguez, B. Salazar-Hernandez, *J. Appl. Phys.* 92 (2002) 5566–5568.
- [39] W. Liu, W. Li, Z. Hu, Z. Tang, X. Tang, *J. Appl. Phys.* 110 (2011) 013901.